

Clutter removal for Wi-Fi-based passive bistatic radar

Laurent Storrer
Université Libre de Bruxelles (ULB)
 Brussels, Belgium
 laurent.storrer@ulb.ac.be

Hasan Can Yildirim
Université Libre de Bruxelles (ULB)
 Brussels, Belgium
 hasan.can.yildirim@vub.be

Claude Desset
IMEC
 Leuven, Belgium
 claude.desset@imec.be

Marc Bauduin
IMEC
 Leuven, Belgium
 marc.bauduin@imec.be

André Bourdoux
IMEC
 Leuven, Belgium
 andre.bourdoux@imec.be

François Horlin
Université Libre de Bruxelles (ULB)
 Brussels, Belgium
 fhorlin@ulb.ac.be

Abstract—We address the problem of static clutter removal in Wi-Fi-based passive bistatic radars. Our goal is to detect slowly moving targets in highly cluttered indoor environments, using Orthogonal Frequency-Division Multiplexing signals from the 802.11n and 802.11ac Wi-Fi standards as sources of opportunity. We propose alternatives to the commonly used Extended Cancellation Algorithm (ECA) clutter removal method. Those alternatives are compared to ECA with simulations using an innovative metric based on CA-CFAR detection, and validated with experimental measurements using two Universal Software Radio Peripherals, along with a fan and an electric train as radar targets. The conclusion of that analysis is that, thanks to the decoupled range and Doppler radar processing, simple novel methods such as Average Removal are efficient alternatives to the computationally intensive ECA which is currently the state-of-the-art in CR.

Index Terms—Passive radars, Wi-Fi, OFDM, Clutter removal, CA-CFAR

I. INTRODUCTION

For many applications, it is useful to perform *indoor monitoring*, *i.e.* to remotely monitor movements of people or objects in buildings. Examples include control of building evacuations and intrusion detection [1], assistance of security staffs in airports or public places [2], or human movements classification [3]. Indoor monitoring with radar is of interest when cameras do not have line-of-sight or cause privacy concerns. Radars can estimate the distance of targets based on signals propagation time (range processing), and the speed of targets thanks to the Doppler effect (Doppler processing).

Furthermore, it is possible to perform indoor monitoring with a minimal budget by using a passive bistatic radar. Bistatic means that the transmitter (TX) and the receiver (RX) are not colocated. Passive means that TX is a non-cooperative source of opportunity. It has been shown in the last years that Wi-Fi signals, based on Orthogonal Frequency-Division Multiplexing (OFDM) modulation, can be an interesting source of opportunity thanks to their quasi-ubiquitous availability [1]. This work focuses on Wi-Fi-based passive radar, in which TX is a non-controlled Wi-Fi access-point and RX is an antenna

capturing a potential direct signal from TX and signal echoes that reflected on targets. The output of the passive radar is a 2D range-Doppler map (RDM) where targets are identified by amplitude peaks. In this work, it is assumed that TX and RX share the same clock to avoid any carrier frequency offset.

Radar processing can be performed in two ways. The classical approach, denoted here as *simultaneous approach*, is to perform range and speed processing simultaneously, usually by means of a 2D cross-correlation function (2D-CCF) [1]. However another approach, denoted here as *decoupled approach*, obtains better results by exploiting the characteristics of OFDM to perform the range processing and the Doppler processing separately [4]. This decoupling also allows to perform range processing with channel estimation techniques from OFDM-based telecommunications, *e.g.* Frequency-Domain Maximum Likelihood channel Estimation (FDMLE) or Time-Domain MLE [5]. With that approach the Doppler processing is performed by a Discrete Fourier Transform (DFT), implemented as a Fast Fourier Transform (FFT)¹, that reveals the Doppler frequency shifts due to the target movement. A window has to be applied prior to this FFT to reduce target leakage, as explained in Section III-C. The *decoupled approach* is followed in this work, and illustrated on Fig. 1.

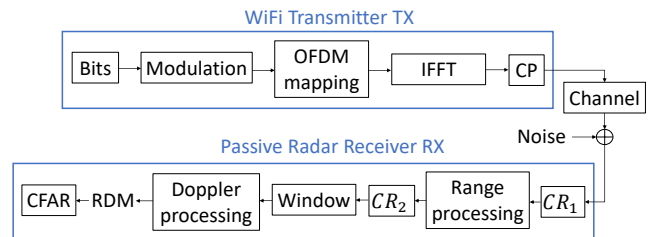


Fig. 1. Passive radar block scheme - Decoupled approach

¹The FFT is used to implement the DFT because it is equivalent and implementation-wise more efficient. This also applies for the Inverse DFT (IDFT), implemented as an Inverse FFT (IFFT).

The challenge addressed in this work is the *clutter removal* (CR). The clutter denotes in this work the unwanted echoes from static objects. They are located at DC (zero Doppler shift because of zero speed) on the RDM. However the windowing prior to the Doppler FFT brings the main problem of clutter removal: if there is no windowing, the DC clutter can be removed easily by just cancelling the DC component after the FFT. However, due to the windowing, the windowed DC clutter features a main lobe that is spread on the low frequency bins (both negative and positive) potentially hiding real targets moving at low speed.

The widely used clutter removal technique is called Extended Cancellation Algorithm (ECA); a method based on least-squares that builds a clutter subspace and projects the received signal on the subspace orthogonal to the clutter [1], [6]. This is mainly used because with the *simultaneous approach*, the user is forced to remove clutter before the 2D-CCF. In the *decoupled approach* illustrated on Fig. 1, ECA would thus take place in the CR_1 block. Enhancements of ECA have been proposed in [7].

The *decoupled approach* allows to apply clutter removal methods of lower complexity than ECA [4]. With this approach, clutter removal is performed between range and speed processing, in the CR_2 block. Our work investigates this track further, by proposing simple clutter removal methods for the *decoupled approach* to further reduce computation complexity, and by extending the comparison with ECA by not only assessing how well clutter is removed but also how clutter removal affects low speed target detection with a Cell Averaging Constant False Alarm Rate (CA-CFAR) detector.

This paper is structured as follows: in Section II and Section III, the system model and radar processing steps are briefly summarized. In Section IV, different clutter removal methods are presented. In Section V, their consequences on the CA-CFAR threshold computation are compared using simulations and their efficiency is assessed on experimental measurements using two Universal Software Radio Peripherals (USRPs).

As a convention, lowercase letters correspond to time-domain signals (e.g. x), and uppercase letters to frequency-domain signals (e.g. X). Bold uppercase letters denote matrices of time-domain signals (e.g. \mathbf{X}), and bold uppercase calligraphic letters denote matrices corresponding to frequency-domain signals (e.g. \mathcal{X}).

II. SYSTEM MODEL

For the sake of simplicity, it is considered that one known OFDM symbol of size Q is transmitted continuously N times, forming a stream of identical symbols. This OFDM symbol can be a field from the Preamble of a 802.11ac Wi-Fi packet [8]. However, no guard bands are used in the OFDM spectrum, this problem being treated separately in [5]. The time-domain known OFDM symbol is the IDFT of known frequency-domain complex QAM or PSK symbols [9]. The transmitted

stream can be represented by a matrix \mathbf{X} where each column, denoted with index k , is one OFDM symbol:

$$\mathbf{X}[i, k] = \frac{1}{Q} \sum_{q=-Q/2}^{Q/2-1} \mathcal{X}[q, k] e^{j2\pi qi/Q} \quad (1)$$

where \mathcal{X} is the matrix of frequency-domain complex QAM or PSK symbols, $q = -\frac{Q}{2}, \dots, \frac{Q}{2} - 1$ is the subcarrier index and $i = 0, 1, \dots, Q - 1$ is the time samples index (often called *fast time* index). The time between two consecutive time samples is defined as $t_s = 1/BW$ where BW is the bandwidth of the system. The column index $k = 0, 1, \dots, N - 1$ refers to the OFDM symbol index (often called *slow time* index). The time between two consecutive OFDM symbols, i.e. the duration of one OFDM symbol, is defined as T .

The environment containing stationary obstacles and moving targets is modelled by a channel impulse response (CIR) discretized into delay bins. The CIR changes between the different OFDM symbols due to Doppler shifts. Hence, the different CIRs, one per OFDM symbol, can be stacked in a matrix \mathbf{H} whose elements are $\mathbf{H}[i, k]$. The distance between TX and the r -th target is defined as $d_{TX,r}$, the distance between the target and RX as $d_{r,RX}$, and the bistatic distance of the target as $d_r = d_{TX,r} + d_{r,RX}$. The CIRs delay bins are [9]:

$$\mathbf{H}[i, k] = \sum_{\tau_r \in \text{bin } i} a_r e^{-j2\pi f_c \tau_r} e^{j2\pi f_r k T} \quad (2)$$

where a_r is the complex amplitude of the multipath component (MPC) reflecting on the r -th target,

$$\tau_r = d_r/c \quad (3)$$

is the propagation delay of this MPC (where c is the speed of light in vacuum) and f_c is the carrier frequency. The propagation delay is discretized with the sampling time t_s , such that the CIRs from (2) contain peaks at indexes $i_r = \left\lfloor \frac{\tau_r}{t_s} \right\rfloor$ for each target r , i.e. at the discrete index being the closest to the continuous delay value. Each delay bin directly corresponds to a distance (range) bin since range and delay are linked by (3). The Doppler frequency shift is here assumed to be maximal to simplify the analysis, thus the bistatic angle of the target [10] is not considered. In this simplified case, with a wavelength λ , the Doppler frequency shift of the r -th target moving at speed v_r is:

$$f_r = \frac{2v_r}{\lambda} \quad (4)$$

Each time-domain received signal is the convolution of one transmitted OFDM symbol with the CIR. This is equivalent to a product in the frequency domain:

$$\mathcal{Y}[q, k] = \mathcal{H}[q, k] \mathcal{X}[q, k] + \mathcal{W}[q, k], \quad (5)$$

where \mathcal{Y} and \mathcal{H} are respectively the matrices of frequency-domain received signal and channel transfer function (CTF) for each transmitted OFDM symbol with index k . \mathcal{W} is a matrix in which each column is the FFT of a i.i.d. sequence of Additive White Gaussian Noise samples.

III. RADAR PROCESSING

A. Range Processing

Range processing consists of computing the bistatic distance, d_r , for each target r . In this work, this is achieved by performing channel estimation, *i.e.* estimating the CIR. The frequency domain CTF is estimated by FDMLE [9] for each OFDM symbol. The estimates can be stacked in a matrix $\hat{\mathcal{H}}$, in the same way as the transmitted signal matrix:

$$\hat{\mathcal{H}}[q, k] = \mathcal{Y}[q, k] / \mathcal{X}[q, k]. \quad (6)$$

The estimated time-domain CIRs are then obtained by an IFFT on each column of $\hat{\mathcal{H}}$, *i.e.* one IFFT per OFDM symbol:

$$\hat{\mathbf{H}}[i, k] = \frac{1}{Q} \sum_{q=-Q/2}^{Q/2-1} \hat{\mathcal{H}}[q, k] e^{j2\pi qi/Q}. \quad (7)$$

$\hat{\mathbf{H}}$ is often denoted as the *range-slow time map* in radar applications. It contains the estimated delay $\hat{\tau}_r$ of each target r , that allows to compute the target bistatic distance $\hat{d}_r = c \hat{\tau}_r$. The range resolution is expressed as $d_{res} = c t_s/2$. The 802.11ac standard allows bandwidth up to 160 MHz, yielding $d_{res} = 0.9375$ m. If the Doppler shift is low, which is the case for low speed targets, the received OFDM symbols can be averaged by groups of M symbols before the channel estimations to reduce the impact of noise [10].

B. Doppler Processing

A length- N FFT is then computed across the channel estimations, *i.e.* across the rows of the range-slow time map $\hat{\mathbf{H}}$, to estimate the Doppler frequency shift of the targets. It yields the already mentioned RDM, denoted $\hat{\mathbf{H}}_D$, whose elements are $\hat{\mathbf{H}}_D[i, n]$, where n is the frequency bin index of the Doppler FFT. The frequency resolution is $f_{res} = \frac{1}{NT}$. The computation of the target speed with (4) has a speed resolution $v_{res} = f_{res}\lambda/2$. More details on Doppler processing can be found in [10].

C. Windowing

Target energy can leak on neighboring frequency bins if its Doppler frequency is not exactly an integer multiple of the frequency resolution. To reduce this leakage, a window is applied, prior to the Doppler FFT, on each row of the range-slow time map: each row is thus multiplied element-wise with the window coefficients vector. A Blackman window is used, because of its efficient reduction of the leakage, at the cost of having a wide main lobe. However, as already explained, due to the windowing the DC clutter is spread on the low frequency bins, potentially hiding real targets moving at low speed. The whole challenge of clutter removal is thus to remove the clutter without affecting low speed targets.

D. CA-CFAR

To separate targets from the noise floor on the RDM, a threshold is applied on each cell of the RDM. The most common technique is CA-CFAR, for which the threshold is based on the noise power estimate $\hat{\sigma}_n^2$ on a band of size D

centered on the RDM cell. Here the band is 1-dimensional along the range dimension of the RDM [10]. The threshold is expressed as $V_T = D (P_{FA}^{-1/D} - 1) \hat{\sigma}_n^2$, where P_{FA} is the probability of false alarm, set here at 10^{-5} . The CA-CFAR thresholds can be stacked in a matrix \mathbf{V}_T , in which each element $\mathbf{V}_T[i, n]$ is the threshold for the RDM cell $\hat{\mathbf{H}}_D[i, n]$. More details on CA-CFAR can be found in [10].

IV. CLUTTER REMOVAL METHODS

A. ECA

ECA is fully described in [6]. The main drawbacks of this method are the complexity of the computation of a large pseudo-inverse matrix, and the fact that the matrix to invert can be badly conditioned, resulting in a loss of precision.

B. Average Removal

Average Removal is the novel technique introduced here to remove clutter before it is windowed, hence before it can hide potential low speed targets. It takes advantage of the *decoupled approach* by subtracting the average of each row i from the range slow time map, *i.e.* the complex mean on each range bin across the channel estimations, before performing the windowing and the Doppler FFT. Indeed the average of a row is equal to the DC value of the FFT of the row, *i.e.* the clutter before windowing. This technique takes place in the CR_2 block of Fig. 1. It has the advantage to offer a much lower computational complexity than ECA, and not to suffer from the conditioning problems mentioned in Section IV-A.

C. Delay Line Canceller

Another alternative that is considered in this work is the use of a highpass filter to remove the clutter before windowing. The simplest approach is to resort to a Delay Line Canceller (DLC) filter, whose impulse response is [11]

$$g[k] = \delta[k] - \delta[k - 1] \quad (8)$$

where $\delta[k]$ denotes the Kronecker delta. It is convolved with each row of the range-slow time map before windowing, *i.e.* on each range bin across channel estimates. Equation (8) implies that only the difference between channel estimation coefficients at slow time index k and at $k - 1$ remains after filtering. Hence the clutter, that is static, is removed. The amplitude of the filter frequency response proves to be equal to [11]

$$|G[n]| = 2 \sin\left(\frac{n\pi}{N}\right). \quad (9)$$

This sinusoidal shape creates a distortion on the RDM, as illustrated later on Fig. 4.

V. PERFORMANCE ANALYSIS

A. Numerical results

Two simulations scenarii are considered to assess the performance of the clutter removal methods. Their parameters are given in Table I. The resulting speed resolution is $v_{res} = 1.0615$ m/s. The carrier frequency was not set in the 5 GHz frequency band to be coherent with the experiments

presented later in Section V-B, for which this band had to be avoided due to potential interference with the public Wi-Fi of the building.

TABLE I
SIMULATION PARAMETERS

f_c	BW	N	M	T	Q
2.3 GHz	160 MHz	15360	240	4 μs	512

1) *Scenario 1, clutter only*: This scenario is used to only assess the clutter attenuation obtained by CR algorithms. In this scenario, only one clutter component is present, and it is successively placed at different distances from RX. Let us denote as P the number of frequency bins occupied by the clutter main lobe around the DC bin. Ideally, the clutter should be entirely removed from the range-Doppler map, so the components of the P bins around the DC bin should have their amplitude reduced to the noise floor. The performance metric is the Root Mean Square Error (RMSE) between the RDM $\hat{\mathbf{H}}_D^{\text{clutter}}$ with clutter processed by clutter removal methods at the clutter range bin i_C on P frequency bins centered around the DC bin and a RDM $\hat{\mathbf{H}}_D^{\text{noise}}$ with only noise (no clutter nor target), as a function of the distance between clutter and RX:

$$RMSE_{CR} = \sqrt{\frac{1}{P} \sum_{n=-P/2}^{P/2} \left| \hat{\mathbf{H}}_D^{\text{clutter}}[i_C, n] - \hat{\mathbf{H}}_D^{\text{noise}}[i_C, n] \right|^2} \quad (10)$$

The result is displayed on Fig. 2. DLC cannot be assessed in this scenario because it distorts the noise floor due to its sinusoidal shape (see (9)), altering the RMSE metric artificially. Average Removal and ECA curves are superimposed and they are at the theoretical noise level, meaning that they cancel the clutter regardless of the distance between it and RX.

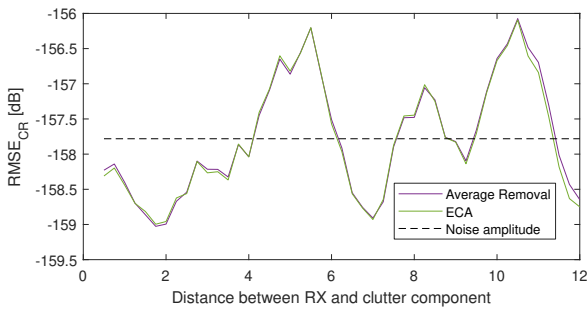


Fig. 2. Comparison scenario 1 - RMSE between clutter and noise amplitude, variable distance

2) *Scenario 2, clutter and target*: This scenario is used to assess how CR affects a low speed target, at range bin i_{tar} and speed bin n_{tar} , in the presence of clutter. Ideally, the target should not be affected by the clutter removal, meaning that its detection by a CA-CFAR detector should not change. The metric used to quantify this is the ratio between the target peak amplitude in the RDM $\hat{\mathbf{H}}_D[i_{tar}, n_{tar}]$ and the CA-CFAR

threshold for this RDM cell, $\mathbf{V}_T[i_{tar}, n_{tar}]$, as a function of the target speed. This ratio is expressed in dB:

$$\eta \text{ [dB]} = 20 \log_{10} \left(\hat{\mathbf{H}}_D[i_{tar}, n_{tar}] / \mathbf{V}_T[i_{tar}, n_{tar}] \right) \quad (11)$$

One clutter component and one target are present at the same range bin $i_{tar} = i_C$. The metric is computed for the case where there is no CR method applied, as a reference, and then for the different cases where CR methods are applied. It is computed for each target speed. Ideally, for each CR method η should be as high as possible and equal or higher than in the case without CR because the target has to be detected without being affected by the CR method. The target is set at 10 m from TX and 9 m from RX. The result of this simulation is displayed on Fig. 3.

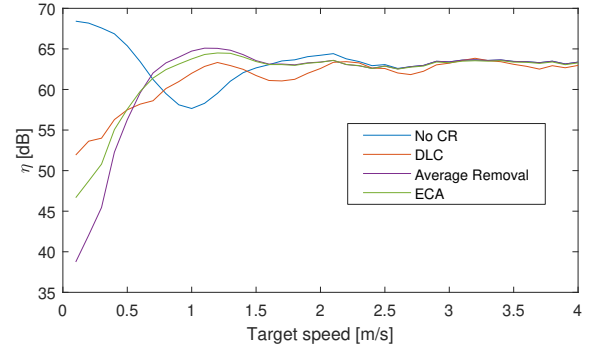


Fig. 3. Comparison scenario 2 - Ratio between target amplitude and CA-CFAR threshold

The first observation is the high value of η , due to two reasons. Firstly, the CA-CFAR threshold $\mathbf{V}_T[i_{tar}, n_{tar}]$ is low w.r.t. the target amplitude due to the limited noise power. Secondly, the averaging combined with the SNR gain of the Doppler FFT yields a high SNR, hence a high $\hat{\mathbf{H}}_D[i_{tar}, n_{tar}] / \mathbf{V}_T[i_{tar}, n_{tar}]$ ratio.

η [dB] is positive, meaning that the target is properly detected. However for target speeds $0 < v < v_{res}$, the target is hidden below the clutter so η without CR is only measuring the clutter. Only with CR the target is properly detected. For target speeds below $v_{res}/2$, η is higher without CR. This is because at those speeds most of the target energy is located at the DC bin and is thus cancelled by CR. However η is still above 0 dB, meaning that the target is still detectable at very low speeds. For those speeds, DLC is the best CR method. For higher target speeds, ECA and Average Removal give a higher and more stable η than the DLC.

B. Experimental measurements

The performance of the clutter removal methods can then be validated by measurements. The experimental setup is detailed in [5]. It consists of two USRPs X310, along with one metallic fan and one electric train as targets. Measurements are performed with custom OFDM signals featuring a bandwidth of 160 MHz. The different components of the targets are highlighted with black rectangles on the top plot of Fig. 4.

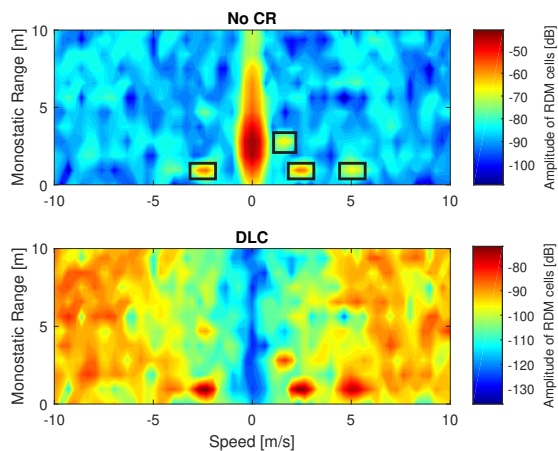


Fig. 4. Measurements RDM - No CR (top) and DLC (bottom)

On the top plot of Fig. 4, no clutter removal was applied and it can be noticed that an important clutter component is present at several range bins. On the bottom plot, DLC was applied. As expected from the sine in (9), it distorts the RDM, yielding high amplitude RDM cells at high speeds. This does not alter the detection process. Indeed, for one Doppler bin, the target and the noise at all range bins undergo the same distortion, meaning that the ratio between target amplitude and CA-CFAR threshold does not vary if the threshold is computed on a one-dimensional band along the range axis. However, since each Doppler bin n is multiplied by a different value of $G[n]$, this distortion prevents the use of the Doppler dimension to estimate the noise for CA-CFAR, and also prevents alternative thresholding approaches, *e.g.* the use of one unique threshold for the whole RDM. More generally, all filtering-based approaches would suffer from this problem. A possible improvement would be to generalize the DLC to a higher order filter to reduce the distortion, so that the filter gain doesn't vary significantly between Doppler bins, except for the DC bin.

On the top and bottom plots of Fig. 5 respectively, ECA and Average Removal are applied. Clutter is properly removed, and both methods give the same visual result.

From this whole comparison of the different clutter removal methods, it can be concluded that Average Removal yields the same performance as ECA, while presenting a much lower computational complexity and avoiding matrix conditioning problems. DLC also gives decent results but has the inconvenience to distort the RDM as illustrated on Fig. 4.

VI. CONCLUSIONS

The separation of range and Doppler processing in Wi-Fi-based passive bistatic radar was exploited to investigate new clutter removal methods yielding lower computational complexity and lower sensitivity to matrix conditioning than the commonly used Extensive Cancellation Algorithm. Those methods were compared to ECA using a standard RMSE metric and a more involved metric related to CA-CFAR detection.

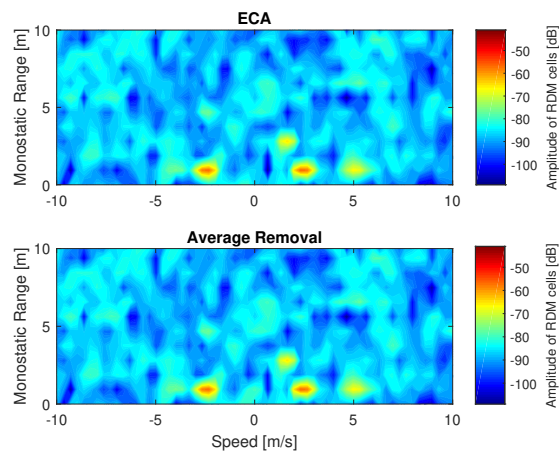


Fig. 5. Measurements RDM - ECA (top) and Average Removal (bottom)

They were also tested on experimental measurements using OFDM signals with a bandwidth of 160 MHz. It turned out that filtering-based clutter removal is a viable approach, yet not suited for all detection methods, and that Average Removal is an efficient low-complexity alternative to ECA.

REFERENCES

- [1] P. Falcone, F. Colone, and P. Lombardo, "Potentialities and challenges of wifi-based passive radar," *IEEE Aerospace and Electronic Systems Magazine*, vol. 27, no. 11, pp. 15–26, November 2012.
- [2] C. Wang, J. Liu, Y. Chen, H. Liu, and Y. Wang, "Towards in-baggage suspicious object detection using commodity wifi," *2018 IEEE Conference on Communications and Network Security (CNS)*, pp. 1–9, 2018.
- [3] B. Tan, K. Woodbridge, and K. Chetty, "A wireless passive radar system for real-time through-wall movement detection," *IEEE Transactions on Aerospace and Electronic Systems*, vol. 52, no. 5, pp. 2596–2603, October 2016.
- [4] L. Fang, X. Wan, G. Fang, F. Cheng, and H. Ke, "Passive detection using orthogonal frequency division multiplex signals of opportunity without multipath clutter cancellation," *IET Radar, Sonar & Navigation*, vol. 10, pp. 516–524(8), March 2016. [Online]. Available: <https://digital-library.theiet.org/content/journals/10.1049/iet-rsn.2015.0238>
- [5] H. Yildirim, L. Storrer, M. Van Eeckhaute, C. Desset, J. Louveaux, and F. Horlin, "Passive radar based on 802.11ac signals for indoor object detection," 2019, Approved for publication at EuRAD 2019.
- [6] F. Colone, D. W. O'Hagan, P. Lombardo, and C. J. Baker, "A multistage processing algorithm for disturbance removal and target detection in passive bistatic radar," *IEEE Transactions on Aerospace and Electronic Systems*, vol. 45, no. 2, pp. 698–722, April 2009.
- [7] C. Schwark and D. Cristallini, "Advanced multipath clutter cancellation in ofdm-based passive radar systems," in *2016 IEEE Radar Conference (RadarConf)*, May 2016, pp. 1–4.
- [8] Aruba Networks, "802.11ac in Depth: White Paper," 2014, Last consultation: June 2019. [Online]. Available: https://www.arubanetworks.com/assets/wp/WP_80211acInDepth.pdf
- [9] Y. S. Cho, J. Kim, W. Y. Yang, and C. G. Kang, *MIMO-OFDM Wireless Communications with MATLAB*. Wiley Publishing, 2010.
- [10] M. Richards, W. Holm, and J. Scheer, *Principles of Modern Radar: Basic Principles*, ser. Electromagnetics and Radar. Institution of Engineering and Technology, 2010. [Online]. Available: <https://books.google.be/books?id=nD7tGAAACAAJ>
- [11] B. Mahafza and A. Elsherbeni, *MATLAB® simulations for radar systems design*. Chapman & Hall/CRC, 01 2003.